JOURNAL OF MATERIALS SCIENCE 28 (1993) 518–528

D.c. and a.c. electrical properties of vacuum evaporated thin SiO/GeO_2 films

C. A. HOGARTH
Department of Physics, Brunel University, Uxbridge, Middlesex, UK
M. H. ISLAM
Department of Physics, Rajshahi University, Bangladesh
A. S. M. S. RAHMAN
Department of Physics, Sultan Qaboos University, Sultanate of Oman

The d.c. and a.c. electrical properties were studied for various compositions of SiO/GeO_2 co-evaporated thin films carrying aluminium electrodes, in the temperature range 193–413 K. A.c. measurements were made over the frequency range 2×10^2–10^6 Hz. The value of the d.c. activation energy was found to decrease with increasing GeO_2 content in the SiO. In the region of high applied field (above 10^6 V m^{-1}), the conduction mechanism is governed by Schottky emission at the blocking contact. The a.c. electrical conductivity, $\sigma(\omega)$, varies with frequency according to the relation $\sigma(\omega) \propto \omega^s$, where the exponent s was found to be dependent on temperature and frequency. The a.c. conduction at low temperature was due to an electronic hopping process. The number of localized sites was estimated from the a.c. measurements for different compositions of SiO/GeO_2 using the models proposed by Elliott and by Pollak, and the values are compared. The Elliott model satisfactorily accounts for the observed a.c. electrical results. A correlation was found between activation energy, optical band gap, conductivity and number of localized sites for the various compositions of SiO/GeO_2 films. The relative dielectric constant, ε_r, and loss factor, tan δ, were found to increase with the increase of GeO_2 content in the films.

1. Introduction

The a.c. transport and dielectric properties of SiO have been studied extensively by many workers during the last three decades due to its interesting properties relevant to the electronics industry. Thin oxide films have also been studied by Argall and Jonscher [1], Hill *et al.* [2], Chan and Loh [3], Frost and Jonscher [4], Goswami and Varma [5], Mahalingam *et al.* [6], Chandra Shakhra and Hari Babu [7], and other workers for similar purposes. Strong evidence of electrical conduction arising from a hopping process in various amorphous materials [8] comes from the frequency dependence of a.c. conductivity in these systems. However, a frequency dependence of a.c. conductivity can also arise from the formation of non-ohmic electrodes [9].

The d.c. electrical properties of GeO_2 and SiO/GeO_2 thin films have been studied by Khan *et al.* [10], and Rahman and Hogarth [11], respectively. These materials show many interesting properties. In these papers some d.c. and a.c. electrical properties of SiO/GeO_2 annealed thin films are reported. The purpose of annealing was to produce stable and reliable assemblies having good reproducible characteristics. The a.c. experimental results have also been compared with theoretical models, given by Pollak [12] and Elliott [13].

2. Experimental procedure

Thin SiO/GeO_2 films were prepared by the co-evaporation technique described by Hogarth and Wright [14]. These oxide materials were evaporated simultaneously from two different sources in the form of tantalum and molybdenum boats, and mixed oxide layers of appropriate thickness were deposited on 7059 Corning glass slides held at a temperature of 100° C in a Balzers BA 510 coating system at an ambient pressure of about 2×10^{-6} torr (1 torr = 133.322 Pa).

Aluminium (for the electrodes) was evaporated from a tungsten coil. Quartz crystals were used to monitor the thickness of the films. The typical evaporation rates for SiO and GeO_2 materials were 1.5 and 0.5 nm s^{-1}, respectively. The insulator thickness was about 300 nm for each composition and the active area of each device was 0.08 cm^2.

Electrical measurements were taken in a vacuum system at a pressure of 10^{-5} torr. The conductance, capacitance and dielectric loss, tan δ, were measured directly with the aid of a Hewlett–Packard Impedance Analyser (5–13 MHz), type 4192A LF. The samples were annealed at 200° C for 2 h inside a measuring system at a pressure of about 10^{-5} torr. While taking measurements, an a.c. signal of 500 $mV_{r.m.s.}$ was applied across the sample. A four-terminal test fixture (model 16047C) supplied with the impedance analyser

0022–2461

was used to minimize the errors in the measurements and zero offset adjustments were also made in the different frequency ranges so as to minimize errors due to parasitic elements in the circuit. Sample temperatures were monitored by an electronic thermometer connected to the sample through a copper/constantan thermocouple. A Solartron (model AS 1411.2 60 V/1A) stabilized power supply unit provided the necessary bias voltage for the d.c. measurements. The current through the sample was measured by an electronic Avometer type EA 113.

3. Results

3.1. D.c. measurements

The voltage–current, V–I, characteristics of several Al–SiO/GeO_2–Al samples having different compositions and a fixed dielectric thickness (300 nm) of SiO/GeO_2 are shown in Fig. 1. It is seen that the conductivity increases with increasing GeO_2 content in the SiO/GeO_2 samples. The V–I curves follow the relation

$$I \propto V^n \tag{1}$$

The conductivities calculated in the low-field region for three different compositions of SiO/GeO_2 are given in Table I. A typical V–I characteristic of an Al–70 mol % SiO/30 mol % GeO_2–Al device at different temperatures is shown in Fig. 2. It is evident that the electric field and temperature both have a profound influence on the magnitude of the electrical conductivity. Fig. 3 shows the plots of $\log I$ versus $1/T$ for various compositions and for various bias voltages. This figure shows an increase in slope with temperature indicating that the activation energy for the conduction process is temperature dependent. The activation energies were calculated using the relation

$$I = I_0 \exp(-\Delta E/kT) \tag{2}$$

where ΔE is the activation energy, k is the Boltzmann constant, T is the absolute temperature and

$$I_0 = e\mu N_d(V/d)A \tag{3}$$

where e is the electronic charge, μ the mobility N_d the impurity or trap density, V the bias voltage, d the insulator thickness, A the active area of the device and I_0 the value of the current extrapolated to $1/T = 0$. The calculated values of the activation energies in the high-temperature region (298–413 K) are given in Table I. It is observed from Table I that the activation energy decreases with the increase of molar percentage of GeO_2 in the SiO. It is common to many amorphous

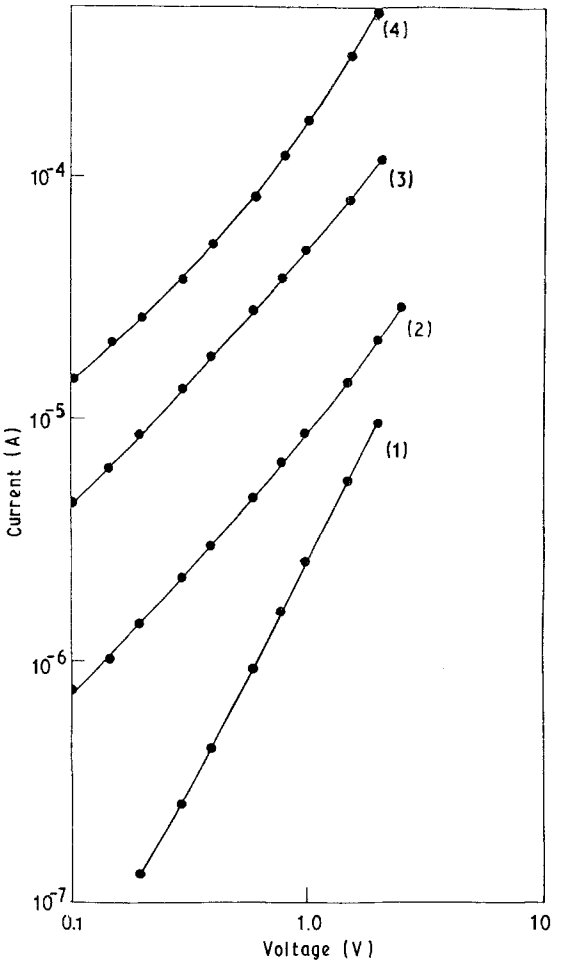

Figure 1 V–I characteristics at room temperature for an Al–SiO/GeO_2–Al device for different compositions of SiO/GeO_2 (thickness ~ 300 nm): (1) 84 mol % SiO/16 mol % GeO_2; (2) 80 mol % SiO/20 mol % GeO_2; (3) 75 mol % SiO/25 mol % GeO_2; (4) 70 mol % SiO/30 mol % GeO_2.

materials that the activation energy is not well-defined because of the absence of sharply defined energy levels [15]. As the temperature increases the carriers become activated from progressively deeper levels, resulting in a steady increase in slope of the log I versus $1/T$ curve. The low values of activation energies (0.10–0.13 eV) at low temperature (223–193 K) are certainly associated with hopping conduction.

The carrier mobility for the three different compositions of SiO/GeO_2 has been calculated in the temperature range 193–223 K using Equation 3 with $d = 300$ nm, $V = 0.4$ V, $A = 0.08\ cm^2$ and assuming the values of N_d from the a.c. measurements. The calculated values of μ are given in Table I. It may be seen that the mobility increases with increasing GeO_2

TABLE I Some electrical and optical parameters of SiO/GeO_2 thin films of different compositions

Film composition (mol %)		Conductivity, σ	Activation energy,	Optical band gap,	Estimated mobility, μ
SiO	GeO_2	$(10^{-9}\ \Omega^{-1}\ cm^{-1})$	ΔE(eV)	$E_{opt}(eV)$	$(10^{-6}\ cm^2\ V^{-1}\ s^{-1})$
84	16	1.86	0.46	2.10	1.61
75	25	18.0	0.38	1.75	25.0
70	30	56.0	0.33	1.60	37.0

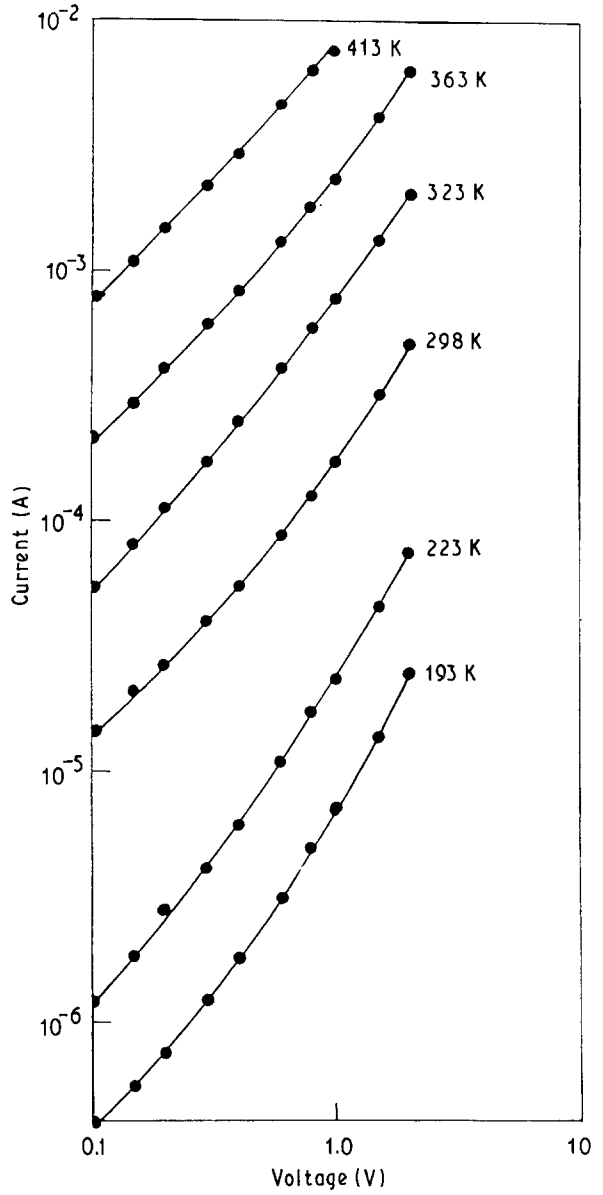

Figure 2 *V–I* characteristics at different temperatures for an Al–70 mol % SiO/30 mol % GeO_2–Al device (insulator thickness ~ 300 nm).

content in the matrix and this low mobility coupled with a low activation energy provides confirmation of hopping conduction at low temperatures.

The d.c. high-field conduction mechanism of SiO/GeO_2 has been reported previously by Rahman and Hogarth [11] who suggested that the conduction mechanism in the high-field region is Schottky emission type at a neutral contact. In the present study, the plots of log I versus $V^{1/2}$ are not good straight lines in the high-field region, as shown in Fig. 4 and the values of the dielectric constant on the assumption of a simple Schottky or Poole–Frenkel effect are inconsistent. The plots of log I versus $V^{1/4}$ show a good straight line (Fig. 5) in the high-field region and give a reasonable value of dielectric constant which indicates that the assumption of a blocking contact leading to a modified form of Schottky emission being the dominant high-field process is a reasonable one for the present samples.

At such contacts a space charge will be created in a depletion region due to the difference in the work function of the metal and of the insulator and if there is an adequate density of traps or donors, N_d (positive when empty), in the insulator, then electrons will be emitted from these states into the metal until thermochemical equilibrium is achieved. This depletion region will extend a distance λ into the dielectric and will give rise to an electric field in this region much higher than the rest of the bulk. This region is more resistive than the rest of the material due to the absence of the mobile charge carriers and the applied potential difference will fall almost entirely across this region.

If this layer has a width λ and the potential drop across it is V_c, then a useful relation governing the emission current is given by Simmons [16]

$$I = AA^*T^2 \exp\left[\frac{8.26\times10^{-6}e(N_d V_c/\varepsilon_r^3)^{1/4} - \phi}{kT}\right] \quad (4)$$

where A is the effective area of the sample, A^* the effective Richardson Dushman constant, T the absolute temperature, k the Boltzmann constant, ε_r the relative dielectric constant, e the electronic charge and ϕ the barrier height.

The electric field, E, and the field-lowering contact-barrier, $\Delta\phi$, are determined by the depletion width, λ, which is in turn determined by the density, N_d, of ionizable impurities according to the relation given by Simmons [9, 16] and Jonscher and Hill [17]

$$\lambda = \left(\frac{2\varepsilon_0\varepsilon_r V_c}{eN_d}\right)^{1/2} = 1052\left(\frac{\varepsilon_r V_c}{N_d}\right)^{1/2} \quad (5)$$

where V_c is the effective potential across the contact, $\varepsilon_0 = 8.854\times10^{-12}\ \mathrm{F\,m^{-1}}$ and $e = 1.6\times10^{-19}$ C.

The electric field at the contact is given by

$$E_c = \left(\frac{2eN_d V_c}{\varepsilon_0\varepsilon_r}\right)^{1/2} = 1.9\times10^{-3}\left(\frac{V_c N_d}{\varepsilon_r}\right)^{1/2} \quad (6)$$

If we assume that the entire applied potential drops across the depletion region, then $V_c = V$ (applied voltage) and a plot of $\log I$ versus $V^{1/4}$ will give a straight line as shown in Fig. 5 of gradient

$$m_b = \frac{\Delta \log I}{\Delta V^{1/4}} = \frac{8.25\times10^{-6}e\log_{10}e}{kT}\left(\frac{N_d}{e\varepsilon_r^3}\right)^{1/4} \quad (7)$$

From Equation 7

$$N_d = 333416\varepsilon_r^3 m_b^4 T^4 \quad (8)$$

From Equation 4

$$\phi = 19.85\times10^{-5}T\left[\log\left(\frac{AA^*T^2}{I_c}\right) + m_b V^{1/4}\right] \quad (9)$$

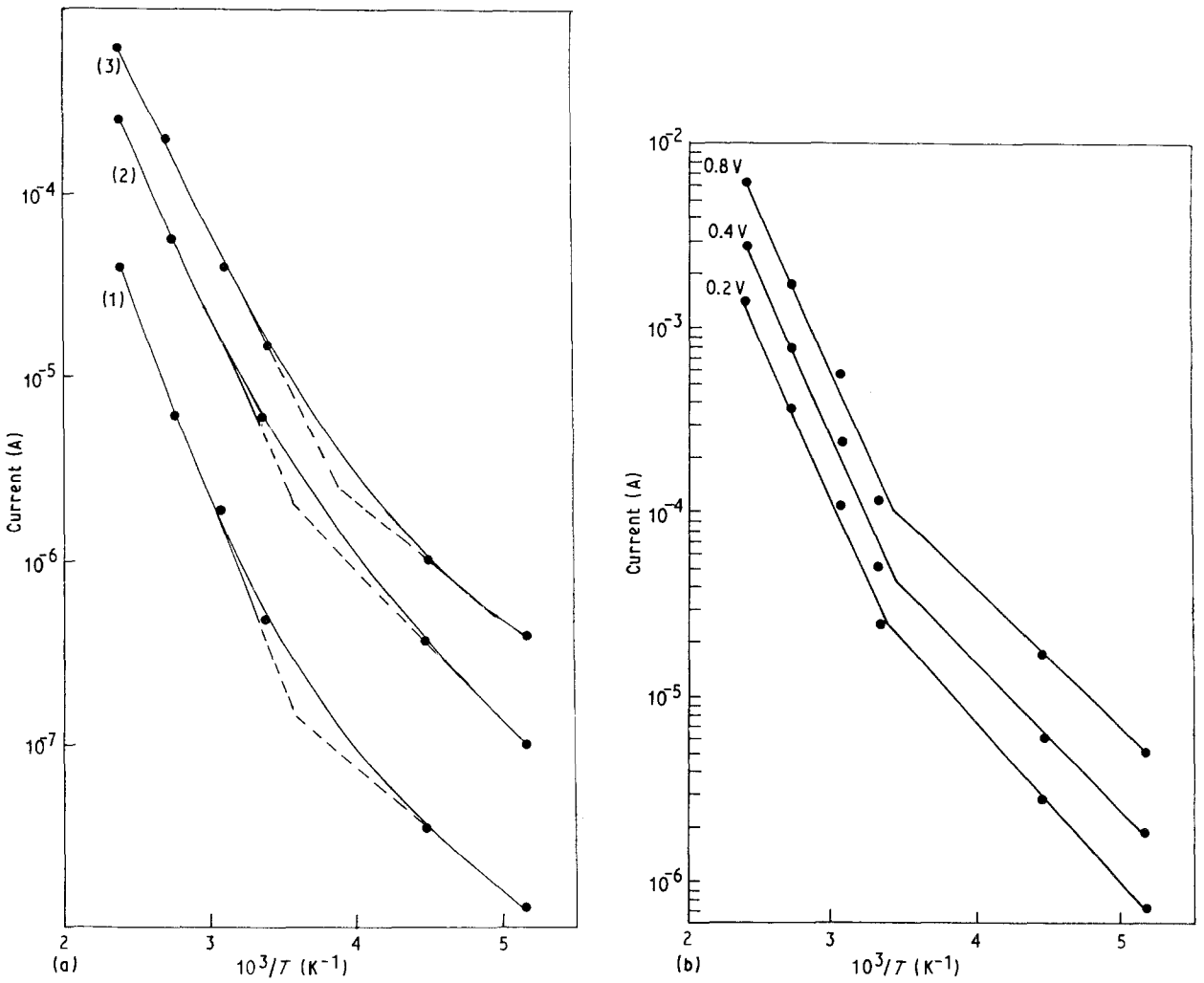

Figure 3(a) Plots of $\log I$ versus $1/T$ at fixed bias voltage (0.4 V) for three different compositions of SiO/GeO_2: (1) 84 mol % SiO/16 mol % GeO_2; (2) 75 mol % SiO/25 mol % GeO_2; (3) 70 mol % SiO/30 mol % GeO_2; (b) Plots of $\log I$ versus $1/T$ for the data of Fig. 1.

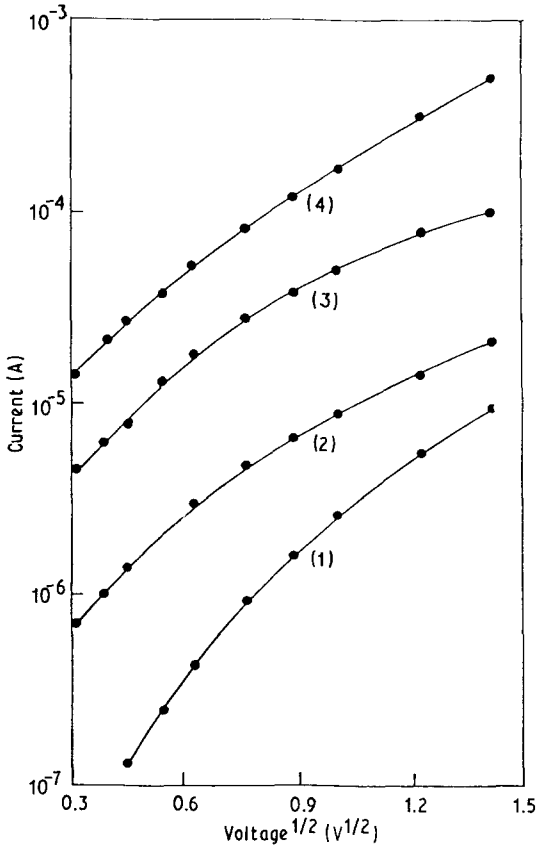

Figure 4 Plots of $\log I$ versus $V^{1/2}$ for the data of Fig. 1.

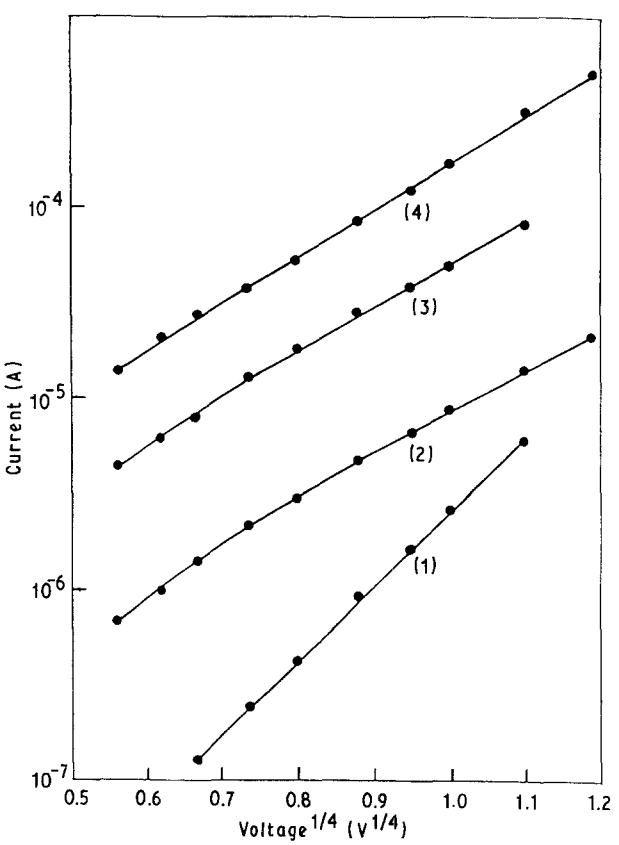

Figure 5 Plots of $\log I$ versus $V^{1/4}$ for the data of Fig. 1.

or at the intercept of $V = 0$, $I = I_0$ and

$$\phi_0 = 19.85 \times 10^{-5} T \log\left(\frac{AA^* T^2}{I_0}\right) \quad (10)$$

The surface density of charge, N_s, per unit area, which is required to screen the internal field, E_c, is given by Jonscher and Hill in the form [17]

$$N_s = \lambda N_d \quad (11)$$

If we assume that the value of $N = 2.29 \times 10^{18}$ cm^{-3} for 70 mol % SiO–30 mol % GeO_2 as calculated from a.c. measurement is a measure of the donor density, N_d, then the value of relative dielectric constant, ε_r, obtained using Equation 8 is 34, which is a reasonable and fairly comparable value in order of magnitude to the high-frequency dielectric constant of 7 (at 1 MHz). For 75 mol % SiO–25 mol % GeO_2 a value of $\varepsilon_r = 2.5$ and a contact barrier height of $\phi_0 = 0.74$ eV are obtained. Using Equations 4–11 and by considering $N_d = 2.29 \times 10^{18}$ cm^{-3} for 70 mol % SiO–30 mol % GeO_2 and at $V_b = 2$ V, the values of $\lambda = 1.7 \times 10^{-6}$ cm, $E_c = 2.35 \times 10^6$ V cm^{-1}, $N_s = 3.89 \times 10^{12}$ cm^2 and the intercept at $V_b = 0$ gives the contact barrier height, $\phi_0 = 0.72$ eV (Table II).

The V–I characteristics at different temperatures for 70 mol % SiO–30 mol % GeO_2 are replotted in terms of a blocking contact associated with the Schottky effect as shown in Fig. 6 and results in a linear dependence of I versus $V^{1/4}$ at the high fields and at different temperatures. The value of the donor density, $N_d = 2.29 \times 10^{18}$ cm^{-3}, is taken from a.c. measurement and is arbitrarily taken as a constant value for determining other parameters. The relative dielectric constant, ε_r, the contact barrier height at zero applied voltage, ϕ_0, the surface density of charge, N_s, per unit area, the depletion width and the electric field at the contact, E_c, have been calculated at different temperatures and are given in Table II. The values of λ and E_c were determined at 2 V. The dependence of ε_r on temperature is plotted in Fig. 7.

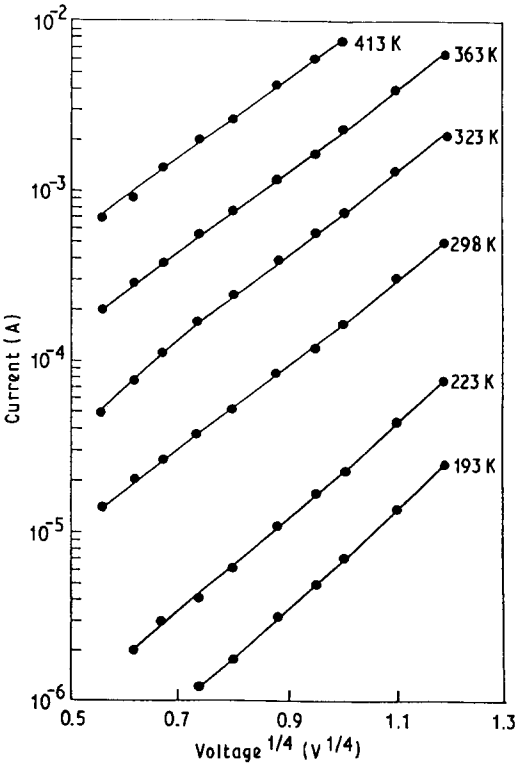

Figure 6 Plots of log I versus $V^{1/4}$ at six different temperatures for an Al–70 mol % SiO/30 mol % GeO_2–Al device of thickness 300 nm.

3.2. A.c. Measurements

The total a.c. conductivity values at different temperatures are plotted against frequency in Fig. 8 for an Al–84 mol % SiO–16 mol % GeO_2–Al device (insulator thickness ~ 300 nm). Fig. 9 shows the plots of total conductance versus frequency at room temperature and low temperature (193 K) for two different compositions of SiO/GeO_2.

The frequency-dependent conductivity is often of the form

$$\sigma(\omega) = \sigma_0 + \sigma_{a.c.}(\omega) \quad (12)$$

which has been observed in many disordered systems. Here σ_0 is the d.c. conductivity and $\sigma_{a.c.}$ (ω) is the frequency-dependent component or "true a.c. conductivity" which is expressed by a relation of the form

$$\sigma_{a.c.}(\omega) = A(T)\omega^{s(T)} \quad (13)$$

where $A(T)$ and exponent $s(T)$ are weakly temperature-dependent parameters and ω is the measuring frequency. The parameter s is also a function of frequency.

From Fig. 8 it is observed that the conductivity increases with frequency for all temperatures. At higher frequencies (above 10^5 Hz) the conductivity increases strongly with frequency tending to ω^2 and is less temperature dependent than in the lower frequency region (below 10^5 Hz). The flattening-off (in the log f curve) at low frequencies as the temperature increases is associated with the increase of d.c. conductivity. The values of the exponent s calculated for

TABLE II Some electrical parameters of a 70 mol % SiO/30 mol % GeO_2 thin-film sample at different temperatures

T (K)	ϕ_0 (eV)	ε_r	N_d (10^{18} cm^{-3})	λ (10^{-6} cm)	N_s (10^{-12} cm^{-2})	E_c (10^6 V cm^{-1})
413	0.86	2.16	2.29	1.44	3.29	2.77
363	0.80	2.28	2.29	1.48	3.39	2.69
323	0.74	2.60	2.29	1.58	3.62	2.52
298	0.72	3.00	2.29	1.70	3.89	2.34
223	0.58	3.70	2.29	1.89	4.33	2.11
193	0.52	3.97	2.29	1.96	4.49	2.04

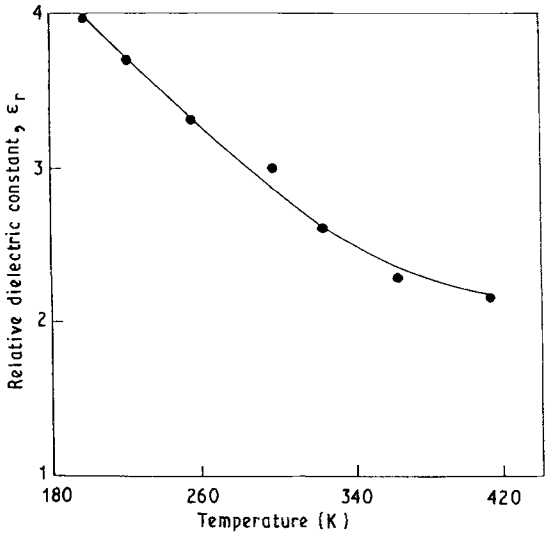

Figure 7 The variation of relative dielectric constant, ε_r, against temperature, T, for an Al–70 mol % SiO/30 mol % GeO_2–Al device.

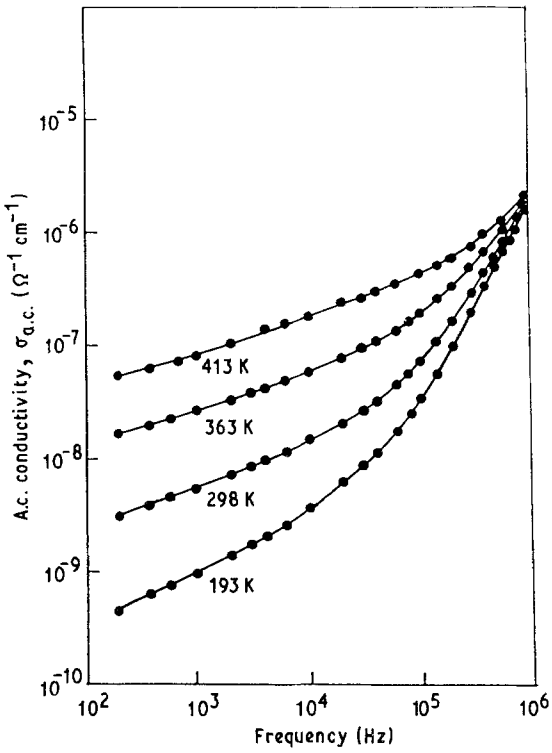

Figure 8 Frequency dependence of the a.c. conductivity of an Al–84 mol % SiO/16 mol % GeO_2–Al sandwich structure (insulator thickness ~ 300 nm) at various temperatures.

different frequency regions and at different temperatures are given in Table III. It is observed from this table that the values of s for the different compositions of SiO/GeO_2 lie between 0.5 and 1 in the 10^2–10^5 Hz frequency range and they increase with decreasing temperature. The value of s seems to be greater than unity at $f > 10^5$ Hz.

Fig. 10 shows the plots of $\log \sigma$ versus $1/T$ for various fixed frequencies and for d.c. This figure shows that as the temperature is increased the a.c. conductivity seems to approach the d.c. conductivity at all frequencies. Consequently, the frequency dependence decreases with increasing temperature as shown in

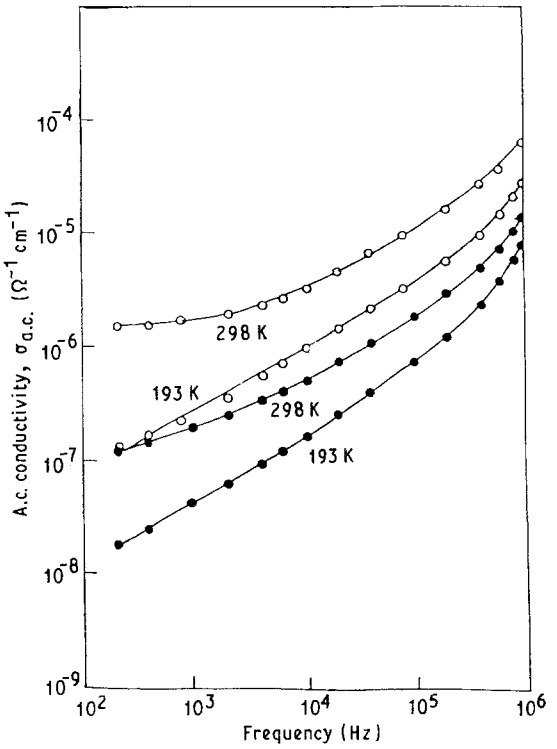

Figure 9 The variation of a.c. conductance with frequency at two different temperatures for two different compositions of SiO/GeO_2. (●) 80 mol % SiO, 20 mol % GeO_2; (○) 70 mol % SiO, 30 mol % GeO_2.

Table III Values of the exponent s at two different temperatures and frequency ranges.

Frequency range (kHz)	Film composition (mol %)		s at	
	SiO	GeO_2	298 K	193 K
20–80	84	16	0.60	0.91
	80	20	0.53	0.63
	70	30	0.54	0.57
100–400	84	16	1.20	1.50
	80	20	0.84	0.94
	70	30	0.81	0.83

Fig. 8. The activation energies for two temperature regions and at different frequencies have been calculated and are tabulated in Table IV. It is observed that the activation energy decreases with the increase of frequency.

The typical variation of capacitance with frequency at different temperatures for an Al–84 mol % SiO–16 mol % GeO_2–Al sample is shown in Fig. 11 and it may be seen that the capacitance is almost frequency independent above 10^4 Hz at all temperatures but at frequencies below 10^4 Hz the capacitance increases with the decrease of frequency and is less pronounced towards lower temperatures. The relative dielectric constant has been calculated using the relation $C = \varepsilon_r' \varepsilon_0 A/d$, where C is the capacitance, ε_r' is the real part of the relative dielectric constant, $\varepsilon_0 = 8.854 \times 10^{-12}$ F m^{-1}, A is the active area of the sample and d is the sample thickness.

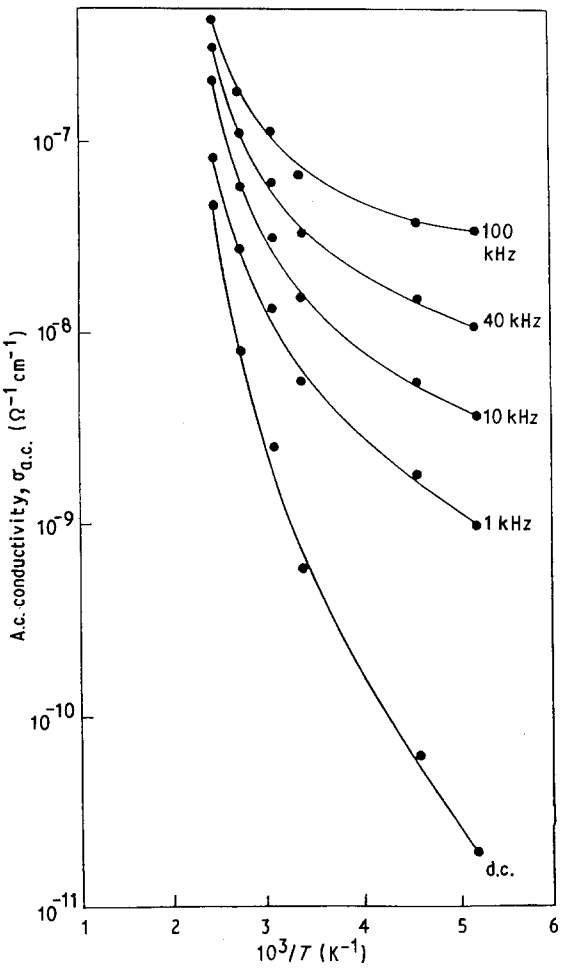

Figure 10 Plots of log $\sigma_{a.c.}$ versus $1/T$ for the data as in Fig. 8.

Fig. 12 shows the plots of the real part of relative dielectric constant, ε_r', versus frequency for three different compositions of SiO/GeO_2. It is observed that the real part of the relative dielectric constant, ε_r', increases with the increasing GeO_2 content in the films. This increase of ε_r' may be associated with the increase of conductivity and a decrease in the spacing of the localized sites [18].

TABLE IV Values of the activation energy, ΔE, at different frequencies and in two different temperature ranges for an Al–84% SiO–16% GeO_2–Al sample.

Frequency (kHz)	Activation energy ΔE(eV) at	
	298–363 K	193–250 K
d.c.	0.32	0.15
1	0.22	0.07
10	0.18	0.05
40	0.14	0.04
100	0.12	0.02

The variation of relative dielectric constant with temperature and at constant frequency is shown in Fig. 13. It shows that the dielectric constant is strongly temperature dependent at lower frequencies and becomes temperature independent when the frequency is above 100 kHz. The dielectric constant at 10 kHz decreased by only 5.6% after annealing of the films at 473 K for 2 h.

Fig. 14 shows the typical variation of tan δ with frequency at different temperatures for an Al–84 mol % SiO–16 mol % GeO_2–Al device. It is seen that each curve shows a $\tan\delta_{min}$ position which shifts to a higher frequency region with increasing temperature, as previously observed in different oxide thin films [2, 5, 19].

The temperature dependence of tan δ at four constant frequencies is shown in Fig. 15. It is seen that tan δ increases with increasing temperature and the variation is more pronounced above 40 kHz but becomes less temperature dependent at 1 MHz.

4. Discussion

It is observed that the activation energy, ΔE, decreases with increasing GeO_2 content in the films and the results are consistent with the decrease of optical band gap, E_{opt} (Table I). This decrease may be explained due to the increase of disorder and the presence of defects

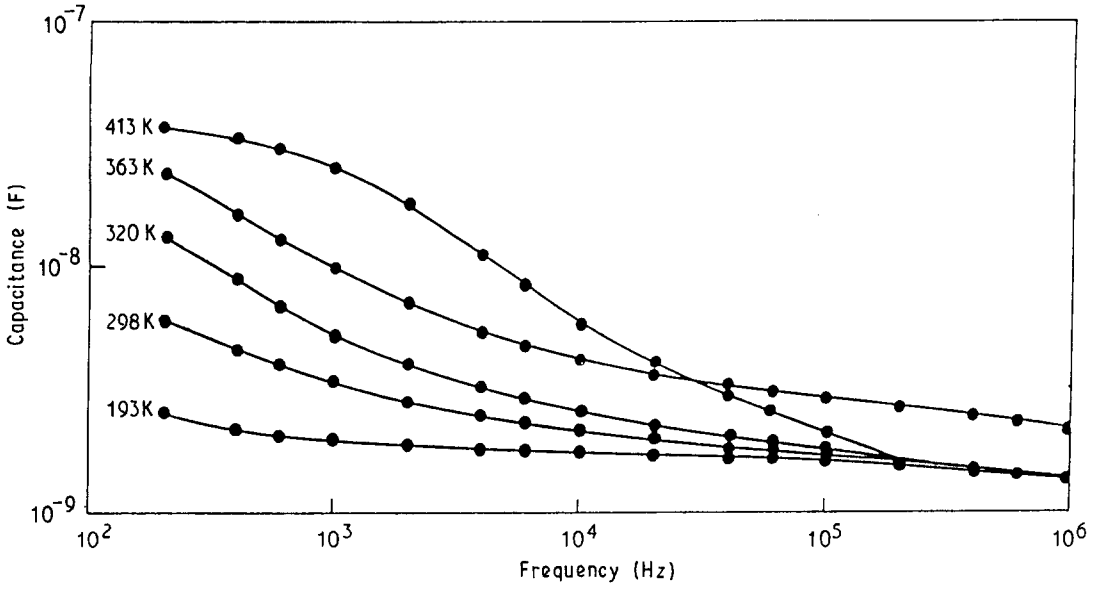

Figure 11 Variation of capacitance with frequency at different temperatures for the same sample as in Fig. 8.

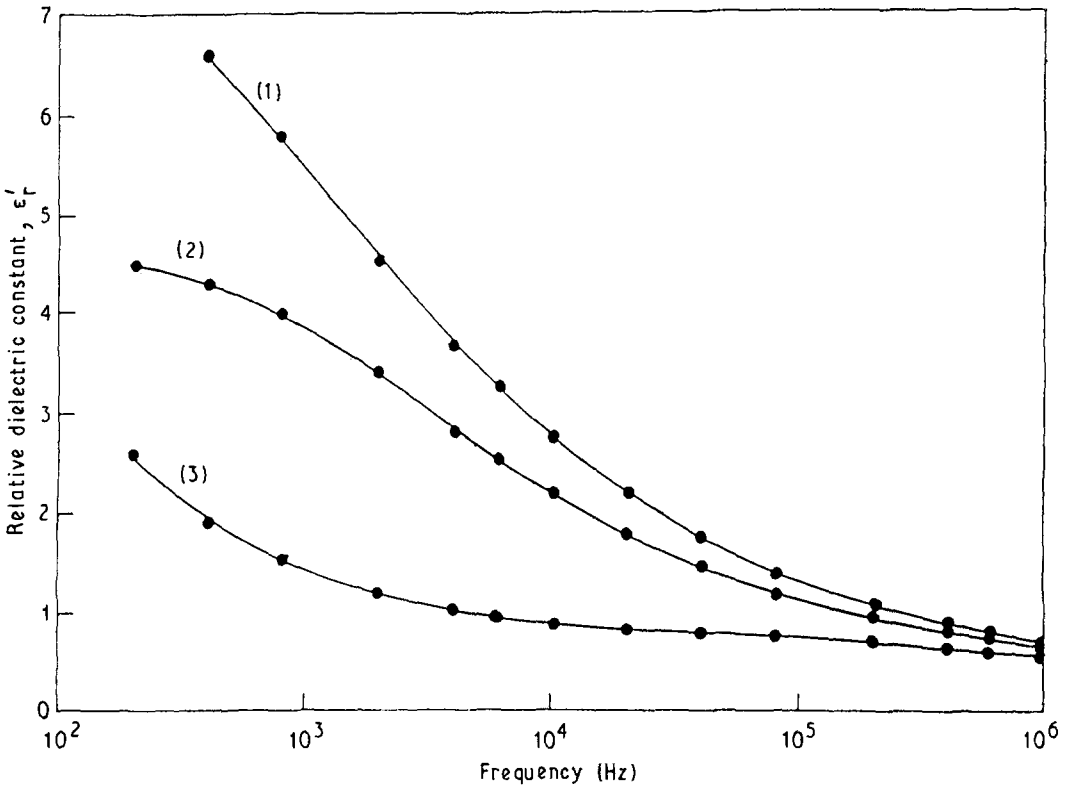

Figure 12 Frequency dependence of the relative dielectric constant for different compositions of SiO/GeO_2 (thickness ~ 300 nm): (1) 70 mol % SiO/30 mol % GeO_2, (2) 75 mol % SiO/25 mol % GeO_2, (3) 70 mol % SiO/30 mol % GeO_2.

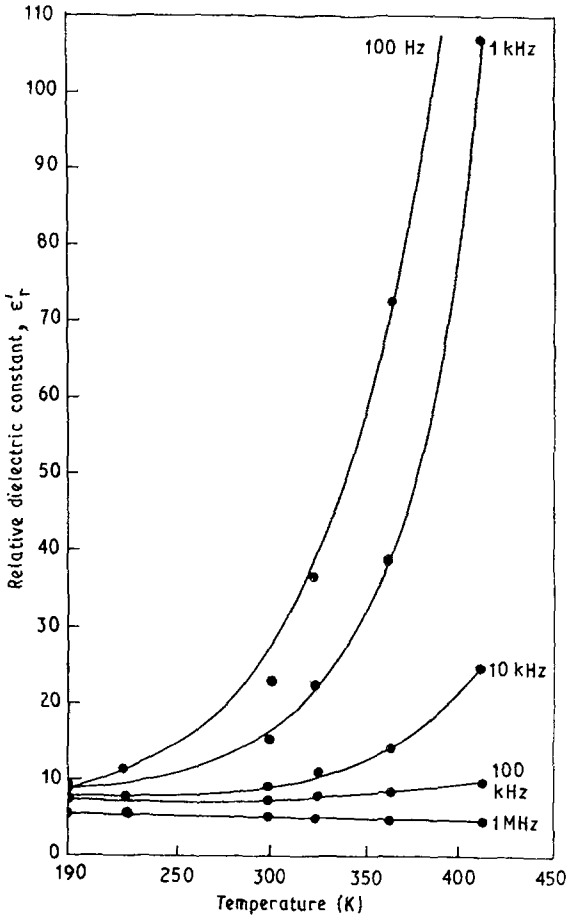

Figure 13 Variation of relative dielectric constant with temperature at various frequencies for the sample as in Fig. 8.

or with the increase in the number of localized sites. The increase of conductivity with increase of GeO_2 content in the samples may be due to the increase of mobility of the charge carriers (Table I). When the density of ionizable centres is high, the height of any barrier present is likely to be small. Accordingly, the values of the barrier height and of ϕ_0 for the two different compositions of SiO/GeO_2 are 0.71 and 0.74 eV, corresponding to N_d values of 2.29×10^{18} and 8.32×10^{17} cm^{-3}, respectively, a result consistent with the barrier height values. In addition, this low value of ϕ_0 is a result of a positive space charge layer in the oxide adjacent to the cathode [20].

It is observed from Table IV that the a.c. activation energy at low temperature is from 0.07–0.02 eV in the frequency range 1–100 kHz. This low value of activation energy coupled with a strong frequency dependence of conductivity tending to a square-law dependence at higher frequencies suggests an electronic hopping conduction process [21]. The square-law dependence of conductivity at higher frequencies may be explained in the following way. As the frequency increases the hops become shorter and in the limit of interatomic distances, will no longer be randomly distributed and thereby will lead to a frequency dependence which tends to ω^2. Similar results have also been observed by Argall and Jonscher [1], Chan and Jonscher [22] and by Owen and Robertson [23] in SiO, Al_2O_3, CS_2 and As_2Se_3. Pollak and Geballe [24] have shown that if hopping takes place between random distributions of localized states, $\sigma \propto \omega^s$, where $0.5 < s < 1$, where the lower value of s occurs for multiple hops, while the higher value occurs for single hops. If hopping takes place between identical sites then $s = 2$ when $\omega < \tau^{-1}$, the characteristic hopping frequency. In addition, Pollak [25] suggests that at higher temperatures, multiple hops occur frequently, while at low temperature single hops

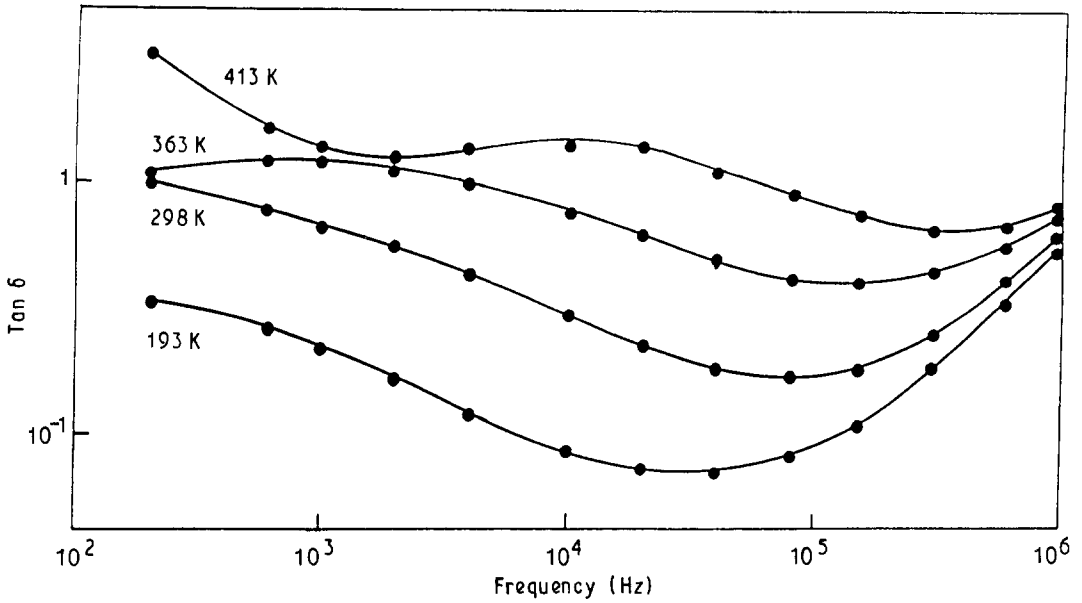

Figure 14 The variation of tan δ as a function of frequency at different temperatures for the sample as in Fig. 8.

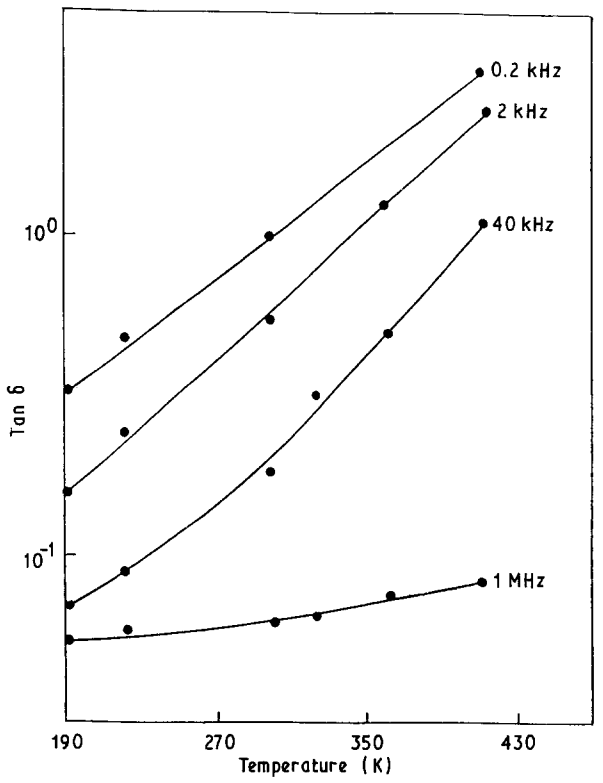

Figure 15 Variation of tan δ with temperature at different frequencies for the same sample as in Fig. 8.

predominate. This leads to an increased thermal activation at high temperatures, with a corresponding decrease in the frequency dependence.

Pollak [12] has derived an expression for the a.c. conductivity (Equation 14) by considering that only those electrons which are in the range of kT at the Fermi level take part in hopping conduction, and also assumes that carrier motion may occur through quantum mechanical tunnelling (QMT) between the localized sites. The following expression has been given by Pollak [12] for uncorrelated hops between pairs of sites

$$\sigma(\omega) = \frac{\pi^3}{96} e^2 kT [N(E_F)]^2 a^5 \omega \left[\ln\left(\frac{1}{\omega\tau_0}\right)\right]^4 \quad (14)$$

where $N(E_F)$ is the density of states at the Fermi level ($cm^{-3} eV^{-1}$), a is the radius of the localized wavefunction, τ_0 is the characteristic relaxation time ($\approx 10^{-13}$ s), k is the Boltzmann constant, ω is the angular frequency and T is the absolute temperature.

The density of localized sites, $N(E_F)$, calculated for three different compositions of SiO/GeO_2 thin films using Equation 14 and taking $a = 0.8$ nm, are given in Table V. The number of sites taking part in conduction for 70 mol % SiO/30 mol % GeO_2 is $N(E_F)kT \approx 1.29 \times 10^{-18}$ cm^{-3}, which is comparable to the value obtained from the Elliott model (Table V).

TABLE V The number of localized sites, $N(cm^{-3})$ and the density of states, $N(E_F)$ ($cm^{-3} eV^{-1}$) for different compositions of SiO/GeO_2 (thickness ~ 300 nm) using the Elliott and the Pollak models. The values have been calculated from the measurements at 100 kHz and assuming that the radius of the localized wave function is a and $\tau_0 = 10^{-13}$ s.

Composition (mol %)		Conductivity, σ (10^{-8} Ω^{-1} cm^{-3})	Relative dielectric constant	Band gap, W_m(eV)	The Pollak model		The Elliott model (10^{18} N cm^{-3})
					$N(E_F)$ (10^{19} $cm^{-3} eV^{-1}$)	N (10^{18} cm^{-3})	
SiO	GeO_2						
84	16	6.9	7.4	2.00	1.8	0.468	0.272
75	25	11.7	11.9	1.75	2.37	0.616	0.832
70	30	51.0	14.5	1.60	4.95	1.29	2.250

It can be seen from Fig. 10 that the slope decreases with decreasing temperature and is also frequency dependent. However, the Pollak equation does not account for the frequency dependence of the exponent s of the frequency dependence of $\sigma_{a.c.}$, as observed experimentally in the present study.

Elliott [13] proposed a theory for a.c. conduction in chalcogenide glasses based on the assumption that carrier motion occurs by means of hopping over the potential barrier separating two defect centres. Although the Elliott model is for chalcogenide glasses, nevertheless it can also be applied to insulating thin films such as As_2Te_3, SiO_2 and SiO/SnO_2 [26–28].

The expression for a.c. conductivity derived by Elliott [13] is given by

$$\sigma(\omega) = \frac{\pi^2 N^2 \varepsilon}{24}\left(\frac{8\varepsilon^2}{\varepsilon W_m}\right)^6 \frac{\omega^s}{\tau_0^{1-s}} \tag{15}$$

where N is the number of localized sites (cm^{-3}), ε is the dielectric constant, W_m is the band gap of the material and the exponent s is given by

$$s = 1 - \frac{6kT}{W_m} \tag{16}$$

Equation 15 can be rewritten in the form

$$\sigma(\omega) = a\omega\left(\frac{1}{\omega\tau_0}\right)^{6kT/W_m} \tag{17}$$

Equation 17 clearly shows the temperature and frequency dependence of conductivity, a is a temperature-independent parameter used in Equation 17.

Thus from Equation 17

$$\frac{d(\ln\sigma)}{d(1/T)} = \frac{6kT^2}{W_m}\ln\left[\frac{1}{\omega\tau_0}\right] \tag{18}$$

From Equation 18 it is observed that the slope decreases as the temperature decreases, in accordance with the experimental observations shown in Fig. 10. In addition, the slope has a frequency dependence. As the frequency, ω, decreases the slope increases for a fixed temperature, again in good agreement with experimental data (Fig. 10). Equation 16 clearly indicates the temperature dependence of the exponent s, which is observed experimentally as shown in Table III. Thus the Elliott model satisfactorily explains the temperature and frequency dependence of a.c. conductivity and the variation of exponent s with temperature. Fig. 10 shows that as the temperature increases the a.c. conductivity seems to approach the d.c. conductivity at all frequencies and the a.c. activation energy is approximately equal to the d.c. value. Elliott [29] suggests that at higher temperatures, another mechanism for $\sigma_{a.c.}$ is predominant, that of excitation to the localized states at the band edges, where conduction takes place instead by quantum mechanical tunnelling.

The concentration of localized sites has been calculated for different compositions of SiO/GeO_2 using Equation 15 derived by Elliott [13] and the results are given in Table V. The values of N are quite reasonable and are comparable to the figure quoted by different authors for amorphous and glassy systems [1, 13, 27, 30]. The values of N decreased by about 3% after annealing of the films. This may be due to the rearrangements of the atoms and to removal of some voids in the matrix. Similar effects have also been observed in different amorphous thin films [31, 32]. It is observed from Table V that the density of localized states $N(E_F)$ increases by a factor of 2.75 with the decrease of the optical band gap 0.5 eV. Austin and Mott [33] suggest that $N(E_F)$ increases with the decrease of mobility gap, due to the greater overlap of the tail states. $N(E_F)$ is also predicted to increase with increasing disorder.

The variation of capacitance, C, $\tan\delta$ and $\tan\delta_{min}$ with temperature can be explained using the model proposed by Goswami and Goswami [34] of a circuit containing an ideal capacitor element of capacitance, C, independent of frequency and temperature, in parallel with a dielectric resistance, R, and in series with a small lead resistance, r, such that $R \gg r$. According to this model, the frequency at which $\tan\delta_{min}$ occurs is

$$\omega_{min} = \frac{1}{C(rR)^{1/2}} \tag{19}$$

and the value of R is

$$R = R_0 \exp\left(\frac{\Delta E}{kT}\right) \tag{20}$$

where R_0 is a constant, ΔE is the activation energy, k is the Boltzmann constant and T is the absolute temperature. Thus R decreases with increasing temperature and, consequently, ω_{min} shifts towards the higher frequency region. It may be noted that the dielectric conductivity is proportional to $\tan\delta$. Therefore, as the temperature increases, the conductivity of the oxide film, and hence $\tan\delta$, would increase.

The absence of a peak in the $\tan\delta$ versus temperature plot (Fig. 15) indicates that the contribution due to dipole orientation would be insignificant [19]. The main contribution to the dielectric constant in the high-frequency region may be due to the electronic polarization. The relative dielectric constant is strongly temperature dependent in the high-temperature region (Fig. 13). This may be related to the fact that at high temperatures the loss is dominated by thermally activated electron hopping whereas in the low-temperature region such an activated process is frozen out, resulting in a decrease of dielectric constant at low temperatures [35].

References

1. F. ARGALL and A. K. JONSCHER, *Thin Solid Films* **2** (1968) 185.
2. A. E. HILL, A. M. PHAHLE and J. H. CALDERWOOD, *ibid.* **5** (1970) 287.
3. S. CHAN and C. K. LOH, *ibid.* **6** (1970) 91.
4. M. S. FROST and A. K. JONSCHER, *ibid.* **29** (1975) 7.
5. A. GOSWAMI and R. R. VARMA, *ibid.* **28** (1975) 157.
6. T. MAHALINGAM, M. RADHAKRISHNAN and C. BALASUBRAMANIAN, *ibid.* **78** (1981) 229.
7. M. CHANDRA SHEKHAR and V. HARI BABU, *J. Mater. Sci. Lett.*, **3** (1984) 600.

8. N. F. MOTT and E. A. DAVIS, "Electronic Processes in Non-Crystalline Materials" (Clarendon, Oxford, 1979).
9. J. A. SIMMONS, G. S. NADKARNI and M. C. LANCASTER, *J. Appl. Phys.* **41** (1970) 538.
10. M. N. KHAN, M. I. KHAN and C. A. HOGARTH, *Phys. Rev. B* **22** (1980) 6155.
11. A. S. M. S. RAHMAN and C. A. HOGARTH, *J. Mater. Sci. Lett.* **5** (1986) 693.
12. M. POLLAK, *Phil. Mag.* **23** (1971) 519.
13. S. R. ELLIOTT, *ibid.* **36** (1977) 1291.
14. C. A. HOGARTH and L. A. WRIGHT, in Proceedings of the International Conference on the Physics of Semiconductors", Moscow, S. M. Ryvkin (ed.) (Nauka, Leningrad, (1968) p. 1271.
15. P. A. WALLEY and A. K. JONSCHER, *Thin Solid Films* **1** (1968) 367.
16. J. G. SIMMONS, "D.C. Conduction in Thin Films" (Mills and Boon, London, (1971) p. 45.
17. A. K. JONSCHER and R. M. HILL, "Physics of Thin Films", (edited by G. Hass, M. H. Francombe and R. W. Hoggman, 1975) p. 169.
18. M. SAYER and A. MANSINGH, *Phys. Rev. B*, **6** (1972) 4629.
19. C. R. DUTTA and K. BARUA, *Thin Solid Films* **100** (1983) 149.
20. S. R. POLLACK, *J. Appl. Phys.* **34** (1963) 877.
21. R. M. HILL and A. K. JONSCHER, *J. Non-Cryst. Solids* **32** (1979) 53.
22. W. S. CHAN and A. K. JONSCHER, *Phys. Status Solidi* **32** (1969) 749.
23. A. E. OWEN and J. M. ROBERTSON, *J. Non-Cryst. Solids* **2** (1970) 40.
24. M. POLLAK and T. H. GEBALLE, *Phys. Rev.* **122** (1961) 1742.
25. M. POLLAK, *Phys. Rev.* **138**A (1965) 1822.
26. H. K. ROCKSTAD, *J. Non-Cryst. Solids* **8–10** (1972) 621.
27. M. MEAUDRE and R. MEAUDRE, *Phil. Mag. B.* **40** (1979) 401.
28. A. S. M. S. RAHMAN, M. H. ISLAM and C. A. HOGARTH, *Int. J. Electron.* **62** (1987) 685.
29. S. R. ELLIOTT, *Phil. Mag. B* **37** (1978) 553.
30. K. L. CHOPRA and C. K. BAHL, *Phys. Rev. B.* **1** (1970) 2545.
31. N. BLUZER and S. K. BAHL, in "Amorphous and Liquid Semiconductors", Vol. 2, edited by J. Stuke and W. Brenig (Taylor and Francis, London, 1974) p. 1209.
32. W. E. SPEAR, in "Amorphous and Liquid Semiconductors," Vol. 1, edited by J. Stuke and W. Brenig (Taylor and Francis, London, 1974) p. 1.
33. G. AUSTIN and N. F. MOTT, *Adv. Phys.* **18** (1969) 41.
34. A. GOSWAMI and A. P. GOSWAMI, *Thin Solid Films* **16** (1973) 175.
35. A. R. LONG and W. R. HOGG, *J. Non-Cryst. Solids* **59–60** (1983) 1095.

Received 2 March
and accepted 30 March 1992